JOURNAL OF GEOPHYSICAL RESEARCH, VOL. 106, NO. A12, PAGES 30,239–30,252, DECEMBER 1, 2001

An overview of observations by the Cassini radio and plasma wave investigation at Earth

W. S. Kurth,[1] G. B. Hospodarsky,[1] D. A. Gurnett,[1] M. L. Kaiser,[2] J.-E. Wahlund,[3] A. Roux,[4] P. Canu,[4] P. Zarka,[5] and Y. Tokarev[6]

Abstract. On August 18, 1999, the Cassini spacecraft flew by Earth at an altitude of 1186 km on its way to Saturn. Although the flyby was performed exclusively to provide the spacecraft with sufficient velocity to get to Saturn, the radio and plasma wave science (RPWS) instrument, along with several others, was operated to gain valuable calibration data and to validate the operation of a number of capabilities. In addition, an opportunity to study the terrestrial radio and plasma wave environment with a highly capable instrument on a swift fly-through of the magnetosphere was afforded by the encounter. This paper provides an overview of the RPWS observations at Earth, including the identification of a number of magnetospheric plasma wave modes, an accurate measurement of the plasma density over a significant portion of the trajectory using the natural wave spectrum in addition to a relaxation sounder and Langmuir probe, the detection of natural and human-produced radio emissions, and the validation of the capability to measure the wave normal angle and Poynting flux of whistler-mode chorus emissions. The results include the observation of a double-banded structure at closest approach including a band of Cerenkov emission bounded by electron plasma and upper hybrid frequencies and an electron cyclotron harmonic band just above the second harmonic of the electron cyclotron frequency. In the near-Earth plasma sheet, evidence for electron phase space holes is observed, similar to those first reported by Geotail in the magnetotail. The wave normal analysis confirms the Polar result that chorus is generated very close to the magnetic equator and propagates to higher latitudes. The integrated power flux of auroral kilometric radiation is also used to identify a series of substorms observed during the outbound passage through the magnetotail.

1. Introduction

The Cassini orbiter carries a comprehensive suite of fields and particles instruments, remote sensing instruments, and the Huygens probe which will be dropped onto Titan. As part of its trajectory to Saturn, the spacecraft performs two flybys of Venus and one each of Earth and Jupiter. The Earth flyby on August 18, 1999, provided the only opportunity for the fields and particles instruments to be operated well within a planetary magnetosphere prior to arrival at Saturn in July 2004. As such, this flyby was utilized for calibrations and checkout of the fields and particles instruments. The Cassini radio and plasma wave science (RPWS) investigation participated in this activity and obtained measurements from August 15 through September 14 as it passed from a location from 593 R_E upstream of the Earth to ~6374 R_E downstream. The primary goals for the RPWS during the flyby were (1) to validate the wave normal analysis capability of the instrument using a five-channel waveform receiver in a regime where whistler mode emissions with well-known characteristics are present and (2) to perform direction-finding observations of auroral kilometric radiation in preparation for a major calibration of that capability at Jupiter. Both the sounder and Langmuir probe portions of the RPWS were also exercised, providing the first opportunity to test their operation in a magnetospheric environment in which they were designed to function. However, the Earth flyby provided a bonus in the form of a comprehensive set of wave data during the flyby. These observations are rare in that such flybys are seldom done at Earth, where orbiting spacecraft are the norm. While orbiting missions are far more useful for magnetospheric studies because of their ability to map the magnetosphere and to provide a long baseline for studying temporal variations and dynamics, an occasional flyby is useful (1) to enable a rapid transit of the entire magnetosphere within just a few hours, not much longer than the typical auroral substorm timescale, and (2) to enable specific comparisons to be made between the eventual Saturn observations and the more familiar terrestrial phenomenology with the same instrumentation.

The RPWS instrumentation is described in detail by D. A. Gurnett et al. (The Cassini radio and plasma wave science investigation, submitted to *Space Science Reviews*, 2000). Briefly, however, the instrument includes three monopole electric antenna elements including two which can be used together as a dipole, a set of triaxial search coils, and a Langmuir probe. There are a number of receivers incorporated into the RPWS. A high-frequency receiver covers the frequency range from 3.5 kHz to 16 MHz with a wide range of variability for

[1]Department of Physics and Astronomy, University of Iowa, Iowa City, Iowa.
[2]Goddard Space Flight Center, Greenbelt, Maryland.
[3]Swedish Institute of Space Physics, Uppsala, Sweden.
[4]Centre d'Etude des Environnements et Planétaires, Université de Versailles Saint-Quentin-en-Yvelines, Velizy, France.
[5]Observatoire de Paris, Meudon, France.
[6]Radiophysical Research Institute, Nizhny Novgorod, Russia.

Paper number 2001JA900033.
0148-0227/01/2001JA900033$09.00

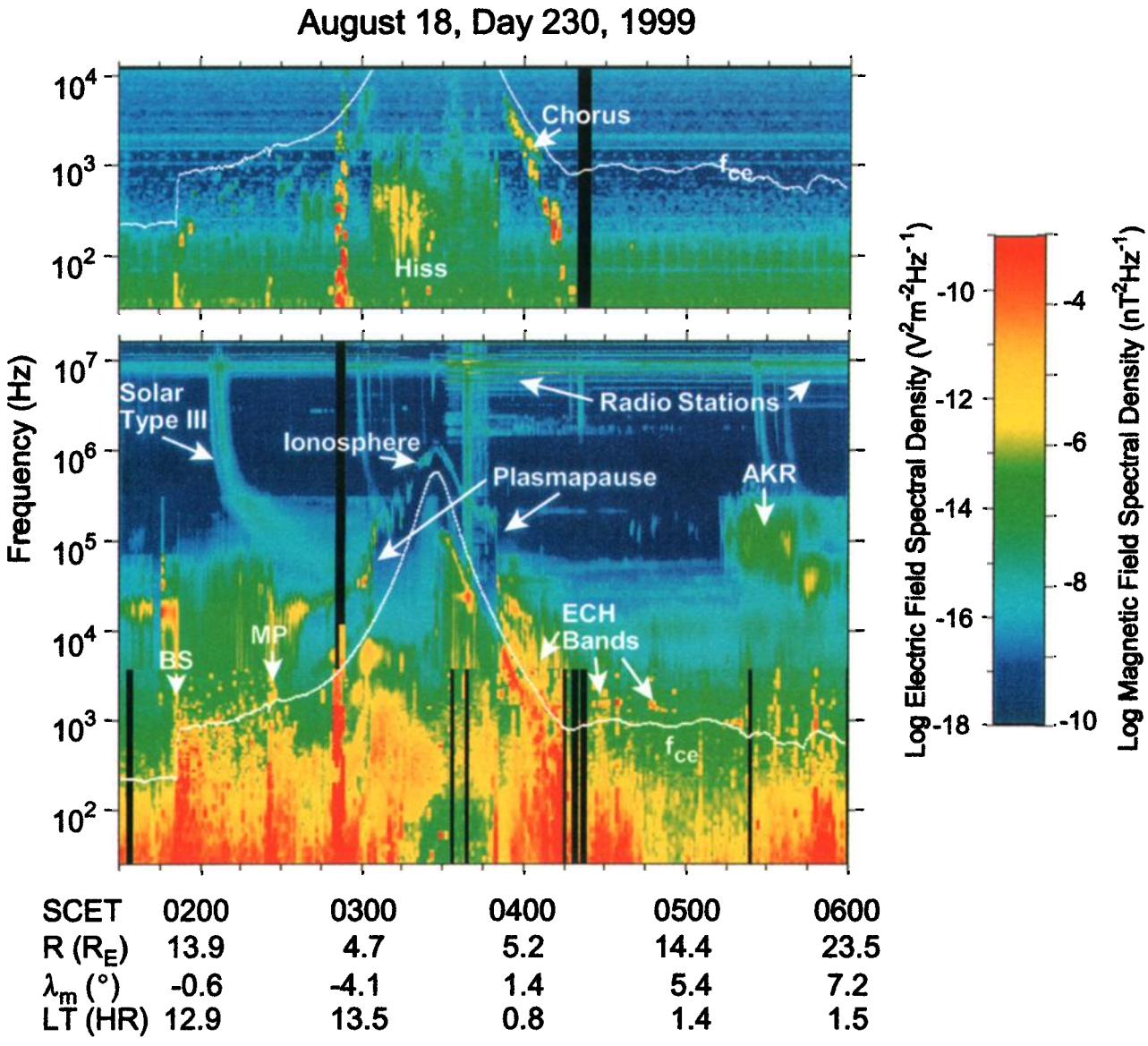

Plate 1. An overview of the magnetic and electric field spectrum observed by the Cassini radio and plasma wave science (RPWS) during the Earth flyby. AKR, auroral kilometric radiation; ECH, electron cyclotron harmonic.

spectral and temporal resolution, time constants, and frequency coverage. It can obtain spectral information only, or it can obtain both autocorrelation and cross-correlation information required to measure all four Stokes parameters and direction-of-arrival information for electromagnetic waves. The Stokes parameters [*Stokes*, 1852] are used to describe partially polarized radiation. S is the total power. Q represents the difference between two orthogonal power components. U and V are basically the cross-correlation functions of the two components of the electric field. From these, the degree of polarization, whether the wave is left- or right-hand-polarized, and the degree to which the wave is linearly or circularly polarized (elliptical polarization) can be determined. See *Krause* [1966] for a complete discussion of the Stokes parameters. The high-frequency receiver includes a sounder for active determination of the local plasma density. The high-frequency receiver utilizes only the three electric antennas. The medium-frequency receiver returns only spectral information from either an electric sensor or a magnetic search coil or, typically, both. It covers the frequency range from 24 Hz to 12 kHz. The five-channel waveform receiver can acquire signals from up to five sensors simultaneously, typically from two electric and three magnetic antennas, and is primarily used for wave normal analyses. It has two frequency ranges including 1–26 Hz and 3 Hz to 2.5 kHz. The low-frequency mode is used to capture waveforms from one electric and one magnetic sensor which are Fourier transformed on board to provide spectral information below 26 Hz to complete the survey spectral information when used in conjunction with the high- and medium-frequency receivers. A wideband receiver enables high duty cycle waveform observations from one of the sensors (selectable) in either a 10.5- or 75-kHz bandwidth. Signals can be downconverted from the high-frequency receiver enabling 25-kHz bandwidth wideband measurements selectable within the

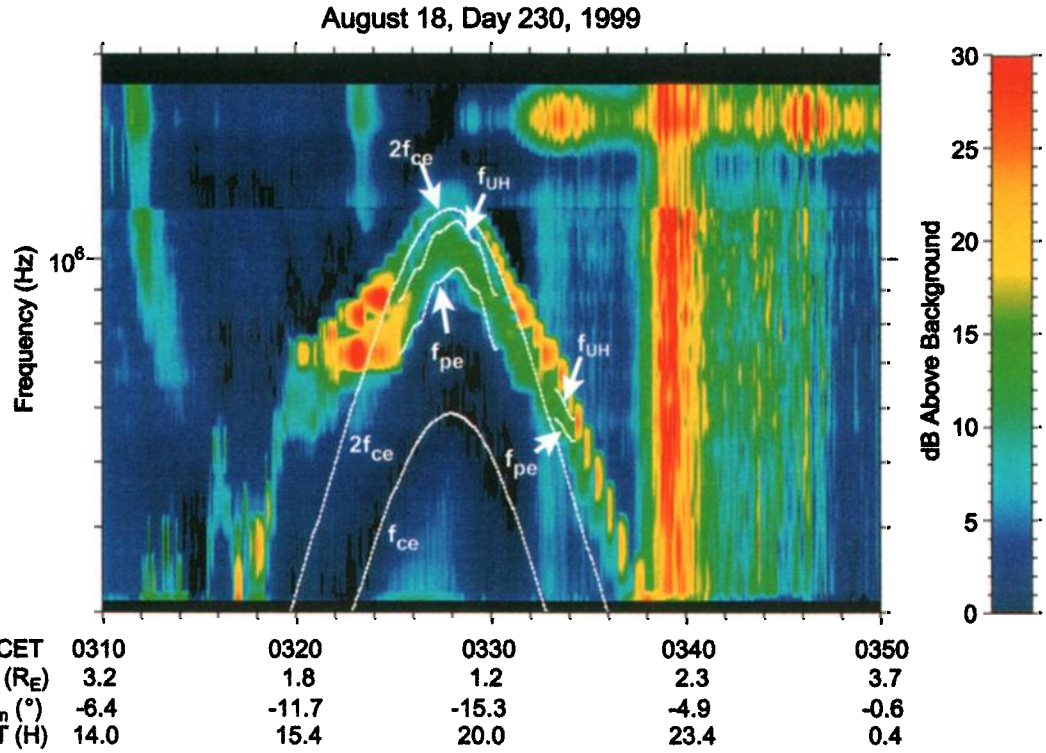

Plate 2. An expanded spectrogram showing details of the plasma wave spectrum near closest approach, particularly the existence of two bands. The f_{pe} and f_{UH} profiles are determined using the measured electron density provided by Langmuir probe current-voltage sweeps and the measured magnetic field. The f_{ce} and $2f_{ce}$ profiles are based on the measured magnetic field. We interpret the upper band as the $5f_{ce}/2$ ECH band, and we interpret the lower one as Cerenkov radiation.

range from 125 kHz to 16 MHz. Since the five-channel waveform receiver can also be operated in a single-channel mode, wideband capability is also available in 26-Hz and 2.5-kHz bandwidths. Finally, Langmuir probe electronics are supplied to control the voltage and to measure the current on the dedicated spherical Langmuir probe and two of the cylindrical electric antennas under certain modes of operation.

The Earth flyby trajectory was chosen solely to safely direct Cassini to its rendezvous target at Jupiter as its next way point on its trajectory to Saturn; no science issues were considered in the selection of the near-Earth trajectory. Nevertheless, the flight path provided an excellent pass through the dayside magnetosphere at a local time near 13 hours, a passage through the plasmapause on the duskside, a closest approach at an altitude of 1186 km at a latitude of −23° near 18 hours local time, and a departure trajectory at a local time of ~1.6 hours. The trajectory for the time near closest approach is shown in Figure 1. The bow shock and magnetopause shown in this illustration are located to indicate the approximate locations of the Cassini encounters with these boundaries on the inbound leg; the shapes are only illustrative. The RPWS and other fields and particles instruments remained on until September 14, when the spacecraft was 6374 R_E downstream. For various engineering considerations, continuous data would not have been possible through the aberrated tail position; hence the RPWS was turned off prior to the nominal tail crossing. There is no evidence in the wave data for a distant magnetotail crossing; hence, in this overview we concentrate on the interval plotted in Figure 1 near Earth.

2. Observations

The RPWS observations during the Earth flyby are summarized in Plate 1. The top panel is a magnetic frequency-time spectrogram covering the range from 25 Hz to 12 kHz. Magnetic spectral density is plotted as a function of frequency and time according to the color bar provided in Plate 1. The bottom panel presents the electric field spectral density in a similar format, except that the frequency range extends to 16 MHz. Because the instrument mode used for the flyby was designed to concentrate on the 2.5-kHz waveform measurements required to validate the wave normal analysis of whistler mode waves, the frequency range below 25 Hz was not continuously available during much of this interval. In both panels a white line is used to trace the electron cyclotron frequency, which is useful in organizing a number of the plasma wave phenomena. The electron cyclotron frequency $f_{ce} = 28\ |B|$, where f_{ce} is in hertz and $|B|$ is in nanoteslas, is determined from the measured magnetic field provided by D. Southwood (personal communication, 1999) and the Cassini magnetometer team.

The top panel of Plate 1 shows plasmaspheric hiss and chorus at frequencies below f_{ce}. The hiss is primarily found between ~0305 and 0350 spacecraft event time (SCET). Chorus is most prominent during the outbound portion between ~0350 and 0415 SCET. The broadband bursty event (also seen in the electric spectrogram) at ~0250 SCET is due to intensive operation of the sounder, which can cause self interference with the RPWS. Normally, this aspect of the investigation will be operated on a very low duty cycle, but this ~5-min period

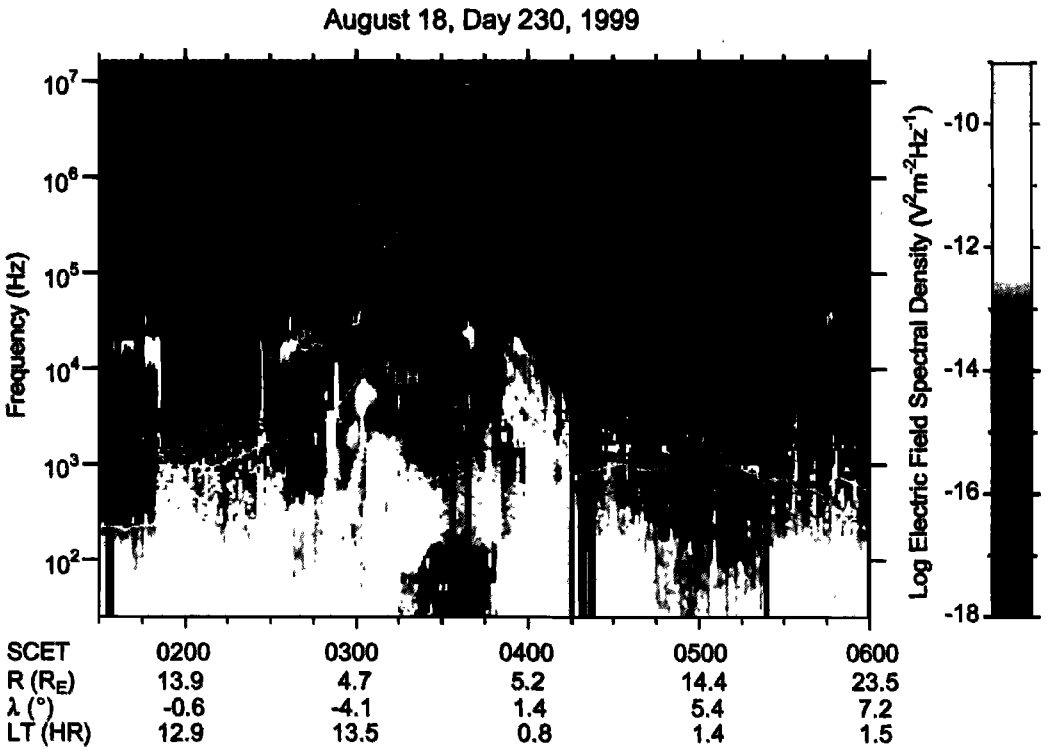

Plate 3. A frequency-time spectrogram showing characteristic frequencies of the plasma. The f_{pe} and f_{UH} profiles are based on the continuum radiation cutoff and the upper hybrid band, respectively. The f_{ce} profile is based on the measured magnetic field, and the f_{LH} frequency is calculated with the assumption of a proton plasma.

was set aside to rapidly vary a number of timing parameters important for the sounder as a means of identifying an optimum configuration prior to arriving at Saturn. Discussion of the results of the sounder will be presented in section 2.3. In addition to the whistler mode emissions seen in the search coil data in the inner magnetosphere, a number of electromagnetic emissions are also seen below f_{ce} near the bow shock, in the magnetosheath, and in the dayside outer magnetosphere.

The bottom panel shows the wealth of radio and plasma wave phenomena expected at Earth. At the highest frequencies are radio emissions of solar and terrestrial origin. The band centered at 8 MHz across the entire spectrogram is due to the one-fourth wave resonance of the E_x dipole antenna. The remaining fixed frequency, narrowband emissions above ~2 MHz are terrestrial radio stations. Notice that the minimum frequency for these bands is significantly lower after closest approach (at 0328 SCET) than it is before. The explanation for this asymmetry is that the ionospheric cutoff over the dayside (inbound) trajectory is much greater than that on the nightside (outbound) trajectory. Such emissions are some of the most obvious characteristics of intelligent life that a flyby spacecraft like Cassini might find at Earth [*Sagan et al.*, 1993; *Kaiser et al.*, 1996]. Solar type III radio emissions are seen sporadically over the time interval plotted in the bottom panel of Plate 1 although the most prominent examples occur at the highest frequencies between ~0205 and 0210 SCET and show strong frequency drifts to lower frequencies with time. This set evolves into a broadband, diffuse emission extending down to tens of kilohertz and is eventually cut off at the plasma frequency in the magnetosphere near 0300 SCET. Auroral kilometric radiation signaling an auroral substorm appears centered on 200 kHz beginning at ~0511 SCET. Continuum radiation trapped in the magnetosphere is a challenge to detect with Cassini's relatively short antennas but can be seen on the dayside between the magnetopause and plasmapause near 20 kHz and on the nightside near 10 kHz between 0430 and 0550 SCET.

The upper hybrid frequency (or Langmuir waves in the solar wind upstream of the bow shock) demarcates the low-frequency limit of radio emissions in Plate 1 and the high-frequency limit of the plasma wave regime. Langmuir waves precede the bow shock at ~20 kHz prior to 0150 SCET. The upper hybrid resonance band can be seen just inside the magnetopause at 0225 SCET, just outside the plasmapause at 0300 SCET, and almost continuously throughout the plasmasphere. The upper hybrid band shows considerable fluctuations in frequency, indicating a highly structured plasmasphere on the dayside. It continues to a peak at ~1 MHz in the ionosphere and drops rather smoothly until the outbound plasmapause crossing near 0350 SCET. More discussion on the interpretation of the emissions in this frequency range near closest approach is given below. The narrowband emissions just above f_{ce} on the outbound leg are electrostatic electron cyclotron harmonic emissions between harmonics of f_{ce}. These emissions continue sporadically after 0415 when f_{ce} flattens out to a nearly constant value near 1 kHz. It is unclear whether the highest-frequency electron cyclotron harmonic (ECH) band beyond the outbound plasmapause is at the upper hybrid resonance or is simply one of the higher $(n + \frac{1}{2})f_{ce}$ harmonics.

A number of quasi-electrostatic and electromagnetic modes are apparent in the bottom panel of Plate 1 below the f_{ce} contour. Both the bow shock and the magnetopause are high-

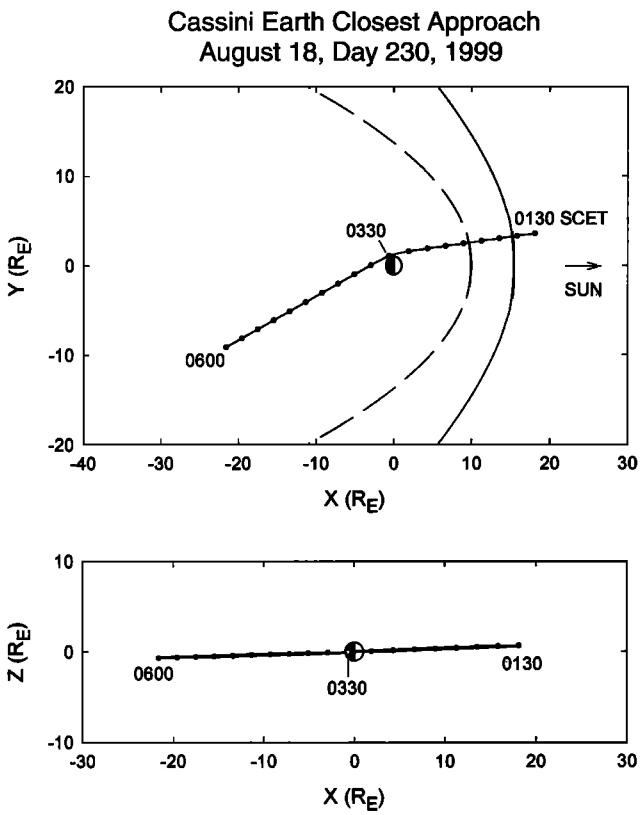

Figure 1. The Cassini flyby trajectory for the region close to Earth showing the observed inbound bow shock and magnetopause crossings. SCET, spacecraft event time.

lighted by broadband wave activity in the electric field spectrum. The magnetosheath is the location of bursty emissions at virtually all frequencies up to the electron cyclotron frequency. Just inside the magnetopause there appears to be broadband electrostatic turbulence, but closer in the emissions become electromagnetic (using the signature in the top panel beginning at ~0235 SCET). Inward, the electric field component of chorus and plasmaspheric hiss is quite strong. The most intense, however, is the band of chorus on the outbound trajectory between ~0350 and 0415 SCET. Broadband electrostatic turbulence is also apparent in this interval, especially at the later times. Broadband electrostatic noise is also apparent beyond 0525 SCET and especially between 0545 and 0555 SCET. There is no indication of a magnetic field component here.

Measurements of natural resonances and cutoffs in the plasma wave spectrum provide a reliable method for determining the plasma density without the perturbing effects of spacecraft potential that can make particle-counting techniques difficult and subject to errors. During the time interval plotted in the bottom panel of Plate 1, both the low-frequency cutoff of continuum radiation at f_{pe} in the dayside outer magnetosphere and the upper hybrid resonance band in the inner magnetosphere are clearly visible. Between the magnetopause and the plasmapause on the inbound portion of the trajectory, we use the low-frequency cutoff of continuum radiation as an indicator of the electron plasma frequency, which is related to the electron density by $f_{pe} = 8980(n_e)^{1/2}$, where n_e is in cm^{-3} and f_{pe} is in hertz. This cutoff is actually an upper limit to the local plasma frequency, since the continuum radiation may suffer a cutoff at some distance from the spacecraft. However, the relatively sharp cutoff suggests that it is local and relevant to the local plasma conditions. The intensification of the upper hybrid band occurs at $f_{UH}^2 = f_{pe}^2 + f_{ce}^2$ and hence is an accurate determination of f_{pe} and hence n_e given that f_{ce} is well known, which it is [*Kurth et al.*, 1979]. However, upon close inspection (Plate 2), the spectrum near f_{UH} is somewhat complex and not immediately interpretable in terms of the location of f_{UH} or other characteristic frequencies of the plasma. We take advantage of the Langmuir probe sweeps performed near closest approach which provide n_e to an estimated accuracy of 10% at several places along the trajectory, approximately once per minute. Using this density and the measured magnetic field, we can draw contours of f_{pe} and f_{UH} on the spectrogram in Plate 2. Interestingly, these bound the broad emission line near closest approach. However, this left the narrower, higher-frequency band without an explanation. Hence we also added a contour at $2f_{ce}$ based on the measured magnetic field. At least for 8–10 min centered on closest approach, this contour lies just below the upper narrowband emission. While not necessarily common in the plasmasphere, the picture in Plate 2 is quite clear and has been reported previously. The broader emission bound by f_{pe} and f_{UH} is Cerenkov radiation between f_{pe} and f_{UH} as noted, for example, by *Taylor and Shawhan* [1974] and *Kurth* [1982]. The narrowband emission is a Bernstein emission, sometimes called an $(n + \frac{1}{2})f_{ce}$ ECH band. For this specific case, $n = 2$; hence this would be the $5f_{ce}/2$ band. While the ECH bands are typically observed between f_{ce} and f_{UH}, it is possible for one or two bands to appear above f_{UH} as reported by *Hubbard and Birmingham* [1978], *Hubbard et al.* [1979], and *Kurth* [1982]. Hence we use this identification to determine f_{UH} (or f_{pe}) near closest approach in determining the electron density profile discussed below. This is an excellent example of the utility of including seemingly redundant techniques for determining plasma density on a spacecraft. Without the independent Langmuir probe assessment an unambiguous identification of the bands at closest approach would have been much more difficult.

The electric spectrogram from Plate 1 is reproduced in Plate 3 for the purposes of showing the use of the low-frequency cutoff of the continuum radiation and the upper hybrid resonance band to determine the electron density along the trajectory. In Plate 3, white traces are used to highlight f_{pe} and f_{UH} as well as f_{ce} and the lower hybrid frequency f_{LH}.

The lower hybrid frequency f_{LH} is a function of both the ion plasma and cyclotron frequencies, f_{ci} and f_{pi}, as well as the electron cyclotron frequency as in (1). For normal conditions the first term on the right-hand side is negligible; hence, to a good approximation, f_{LH} is independent of the plasma density:

$$\frac{1}{f_{LH}^2} = \frac{1}{f_{ci}^2 + f_{pi}^2} + \frac{1}{|f_{ci} f_{ce}|}. \qquad (1)$$

For the trace in Plate 3 we assume a proton plasma.

Using the f_{UH} and f_{pe} profiles in Plate 3, we can produce an electron density profile as shown with lines in Figure 2. The peak ionospheric density encountered was just over 10^4 cm^{-3}. Also plotted in Figure 2 are determinations of the electron density with the sounder and Langmuir probe, discussed in sections 2.3 and 2.4. The structure in the dayside plasmasphere is quite evident with large-scale variations of a factor of 3–5 in density. The inbound plasmapause shows a factor of 30 increase in density. Small-scale variability in the dayside outer magnetosphere is on order of a factor of 2.

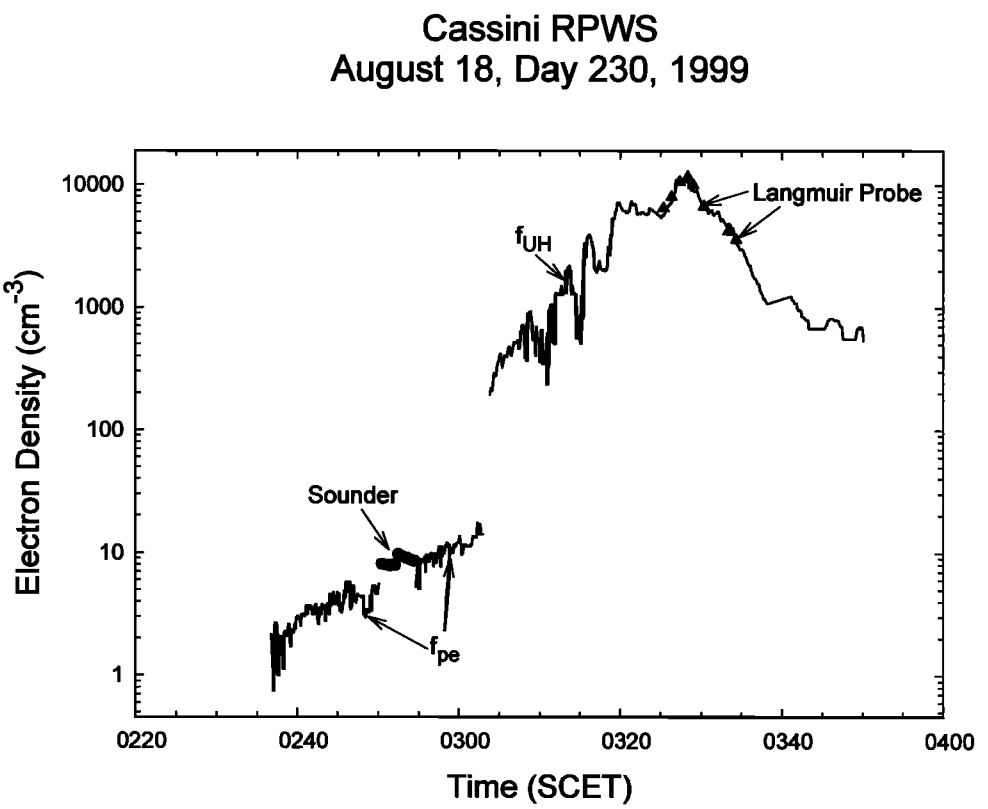

Figure 2. Electron density as a function of time using the measured f_{pe}, f_{UH}, as well as results from the sounder and Langmuir probe.

2.1. High-Resolution Observations

To provide contextual information for the five-channel waveform measurements, the wideband receiver was operated in its 10.5-kHz mode for a nearly 4-hour period centered on closest approach. Because of data volume restrictions, this receiver could only be operated in a relatively low duty cycle mode. In this mode one 2048-point waveform capture was acquired every 375 ms. At the sample rate of 27,777 s^{-1} the duration of the capture is only ~74 ms. Hence the mode affords 74 ms of data per 375 ms for a duty cycle of ~20%. Nevertheless, this mode provided excellent frequency-time information on whistler mode and electrostatic phenomena in the magnetosphere with very high spectral resolution. Plate 4 includes an hour-long portion of this data set beginning near closest approach. The format of Plate 4 is very similar to that of Plates 1 and 2 except that a linear frequency scale is used because the Fourier transform generates linearly spaced spectral components. The electron cyclotron frequency is again superimposed on the spectrogram to separate the whistler mode emissions below f_{ce} from the electrostatic waves above f_{ce}. An intense band of chorus is very prominent between ~0350 and 0410 SCET. There is a gap in the spectrum of the chorus band at $f_{ce}/2$ as is commonly observed. While complex, ECH emissions are seen beginning just above f_{ce}. At least three bands are clearly visible between ~0350 and 0405 SCET, and even more are visible just before the end of the plot at 0430 SCET. Differences in the intensities of the three bands at different times in the earlier interval ensure that the bands are not simply harmonic distortion. This is less clear for those near 0430 SCET.

A particularly interesting feature in Plate 4 is an interval of broadband emissions between ~0410 and 0415 SCET although they are also seen at other times. From inspection of the top panel of Plate 1 it is clear that these emissions are primarily electrostatic in nature. These emissions are examples of broadband electrostatic noise [*Gurnett et al.*, 1976; *Gurnett and Frank*, 1977] which are often found on field lines carrying currents and/or electron or ion beams. On the basis of the realization that such features in Fourier-transformed spectra are actually due to solitary structures [e.g., *Matsumoto et al.*, 1994; *Ergun et al.*, 1998; *Franz et al.*, 1998], we examined the underlying waveforms for this time period. Figure 3 shows a single 74-ms waveform from the 10.5-kHz wideband receiver from 0414:23.2 SCET. Three large-amplitude solitary structures are clearly visible; these are indicative of other waveforms from this interval. The amplitudes of these waves are of order one to a few mV m^{-1}, and the characteristic timescale of the events is ~1 ms. *Franz et al.* [2000] report that the parallel scale size of electron phase space holes is $\sim 2\lambda_D$, where the Debye length $\lambda_D = 11.95\sqrt{T_e/n_e}$ (in centimeters), T_e is the electron temperature in Kelvins, and n_e is the electron density in cm^{-3}. Furthermore, the speed of the electron phase space holes is a fraction of the electron thermal speed $V_e = 6.743 \times 10^5\sqrt{T_e}$ in cm s^{-1}. If we take $2\lambda_D/0.1V_e$, then T_e cancels out and we are left with $2.81 \times 10^3\sqrt{n_e}$ s^{-1} for the characteristic frequency of the structures as seen by an observer at rest. At this time we do not have a good estimate for the electron density; the highest frequency electron cyclotron harmonic emission is at ~5 kHz; hence the minimum plasma frequency at this time cannot be significantly less than this. Hence n_e must be 0.3 cm^{-3} or greater. The characteristic frequency of electron phase space holes then is ~1.6 kHz or the timescale is

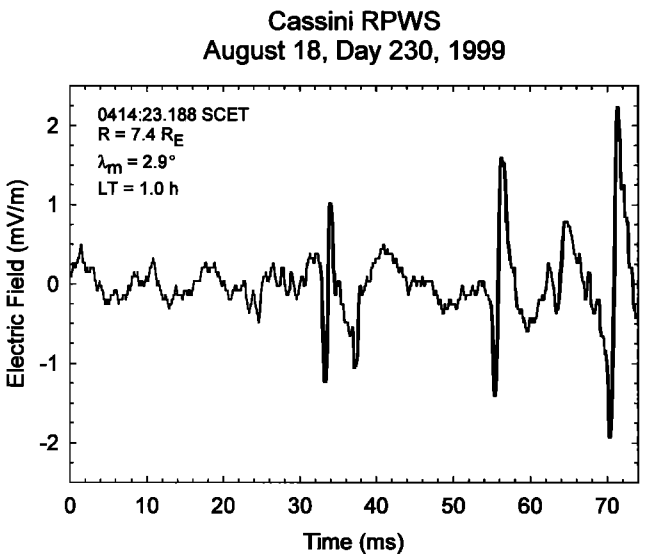

Figure 3. A wideband waveform showing examples of electrostatic solitary structures. The time-scale for these events is consistent with an interpretation as electron phase space holes.

~0.6 ms. This is reasonably close to the observed timescale; hence we are confident in identifying these features as electron phase space holes.

2.2. Wave Normal Analysis

The RPWS utilizes a five-channel waveform receiver to support wave normal analysis of waves in the frequency ranges below 2.5 kHz and 25 Hz. This portion of the instrument simultaneously samples waveforms from the E_x dipole antenna, the E_w monopole extended perpendicular to the dipole, and the triaxial search coils. During the Earth flyby, ~0.29-s-long waveforms were captured once per 20 s for a ~4-hour interval centered on closest approach. We utilize the Means method [*Means*, 1972; *LeDocq et al.*, 1998] to analyze the three magnetic components of waves. This method assumes that the three magnetic components of the waves have a high degree of coherence and are planar. Since this method does not determine the Poynting vector, we solve $\mathbf{S} = \langle \mathbf{E} \times \mathbf{H} \rangle$. However, only two components of **E** are measured, so we use $\mathbf{E} \cdot \mathbf{H} = 0$ to determine the third component of **E**. Plate 5 summarizes the observations and results for the band of chorus shown in Plate 4. In Plate 5a the electric field components are summed to give the electric field spectral density. The magnetic spectral density from the three search coils is given in Plate 5b. Plates 5c and 5d show the results of the wave normal analysis with Θ being the angle with respect to the geomagnetic field and ϕ being the azimuthal angle with 0 defined as the radial direction. Only frequency-time elements for which tests for coherency and coplanarity are satisfied are presented in Plates 5c and 5d. Plate 5e shows the angle of **S** with respect to the geomagnetic field. Finally, Plate 5f shows the sign of $\mathbf{S} \cdot \mathbf{B}$ with red designating positive values, hence indicating that the group velocity is in the direction of **B**. While not shown in Plate 5, the analysis confirms that the chorus waves are right-hand-polarized, as expected. These waves are near the equator just beyond the plasmapause, hence similar to those analyzed by *LeDocq et al.* [1998]. As expected, the chorus emissions have both their wave normal and Poynting vectors nearly parallel to **B** and are right-handed. As explained by *Hospodarsky et al.* [this issue], an analysis of the measured magnetic field for the time period in Plate 5 shows that the true magnetic equator crossing is near 0405 SCET as opposed to 0353 as indicated by the legend at the bottom of the plate, which is based on a simple dipole field model. Therefore the chorus emissions are propagating away from the true magnetic equator as found by *LeDocq et al.* [1998]. Hence we are confident in the ability of the Cassini instrument to obtain the first such results in the Saturnian magnetosphere. *Hospodarsky et al.* [this issue] present the wave normal analysis in greater detail and extend the analysis to whistler-mode waves in the dayside outer magnetosphere and magnetosheath.

2.3. Sounder Observations

The RPWS high-frequency receiver incorporates a relaxation sounder for the purposes of providing the local electron density through the active excitation of characteristic resonances of the local plasma, in particular, the electron plasma frequency, which is directly related to the electron density. Briefly, the sounder operation consists of a 30-V pulse on the dipole antenna, followed by a variable time delay, and then a series of measurements by the receiver at the pulsed frequency with another variable time delay between measurements. After yet a third variable time delay, the next frequency pulse is emitted, and the process is repeated over the range from 4 to 115 kHz. The various time delays are typically on the order of a few to 15 ms. Part of the reason for the operation at Earth was to investigate several sets of time delays to determine a preliminary set to use for Saturn tour planning. The analysis, then, consists of looking for spectral peaks in the measured spectrum which are excited at the electron plasma frequency. Figure 4 shows a sample spectrum with a peak highlighted which has been determined to be the electron plasma frequency excited by the sounder. The frequency of the line is 27.6 kHz, corresponding to an electron density of 9.4 cm^{-3}. Generally, the sounder generated one or more peaks in the received spectrum, with the additional lines being at harmonics of f_{ce} or at the f_q resonances. The analysis is also complicated somewhat by the presence of naturally occurring emissions at f_{UH} during the interval; however, in most cases the triggered emission was at a larger amplitude than the naturally occurring

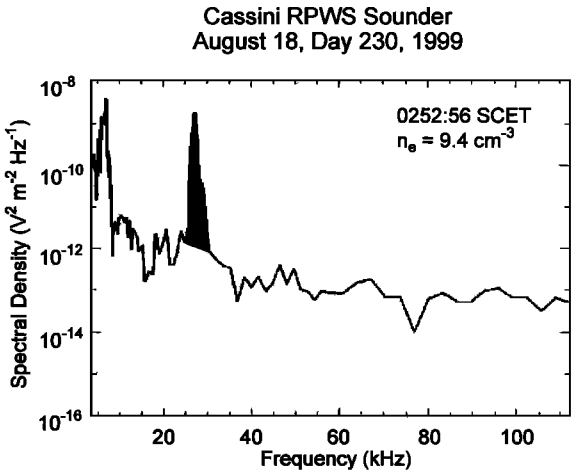

Figure 4. An example of a spectrum including a triggered enhancement at the electron plasma frequency stimulated by the RPWS sounder.

one. Electron densities determined using the sounder results are plotted in Figure 2. The sounder test was generally successful. It indicated that at least for the conditions encountered in a short (~5-min) interval in the terrestrial magnetosphere, the time delay between the pulse and the first receiver measurement must be small, less than 10 ms. However, there is a finite time for the receiver automatic gain control to recover from the pulse (the receiver is not blanked during the pulse), and this argues for delay times which are not too short. This effect is more of a factor for the lowest high-frequency receiver band (3.5–7.2 kHz).

The intended operation at Saturn is to use the sounder for density measurements in the magnetosphere with relatively low duty cycle (primarily because of the potential for interference with RPWS and other instruments' measurements). Nevertheless, these will be very important for providing density information where there are no naturally occurring emissions at f_{pe} or f_{UH}.

2.4. Langmuir Probe Observations

The Langmuir probe was included in the RPWS investigation primarily to provide thermal plasma measurements (electron density and temperature) in Titan's ionosphere, but it is likely that the probe will also be useful in the inner plasma sheet and near the icy satellites. The passage through Earth's ionosphere provided the only opportunity to operate the Langmuir probe in a cool, dense plasma prior to arriving at Saturn. Hence the probe was set to do typical voltage sweeps once per minute for ~10 min near closest approach. In between the sweeps the probe was left in a current-collection mode designed to enable rapid density measurements between the sweeps, assuming the appropriate bias voltage for such measurements would not change drastically between sweeps.

Figure 5 shows a current-voltage curve for one of the sweeps performed at 0326:19 SCET at a radial distance of 1.22 R_E. The uppermost curve shows both the data and a model of the total current; there is virtually no difference between the two, so they appear as a single curve. The voltage is swept both up and down by the Langmuir probe electronics, and there was no indication of any hysteresis between the upgoing and downgoing sweeps. This excellent performance is due in part to the use of TiN as a coating for the 5-cm spherical probe. The other curves represent models of the various constituents of the current. In the negative bias portion of the curve (left-hand side) we have modeled the plasma as consisting of two ion species, O^+ and H^+ with a number density ratio of $N_O{}^+/N_H{}^+ = 0.34$. Of course, the Langmuir probe obtains no information on composition; at Titan such modeling would use the measured ion composition as determined by either the Ion and Neutral Mass Spectrometer (INMS) or the Cassini Plasma Spectrometer (CAPS) instrument. However, given a mass composition, the model can then determine an effective ion temperature, which in this example is 0.05 eV. In the positive bias portion of Figure 5 (right-hand side) the current is primarily due to plasma electrons, but provision is made in the model for photoelectrons from both the spacecraft and the probe itself. Data obtained in early 1999 in the solar wind where the plasma density is much lower and the photoelectron current is significant showed that these two populations of photoelectrons could, indeed, be differentiated. For this example the electron density is 8000 cm^{-3}, and the electron temperature is 0.33 eV. The model also provides an estimate of the spacecraft potential (−0.7 V in this example) and an estimate

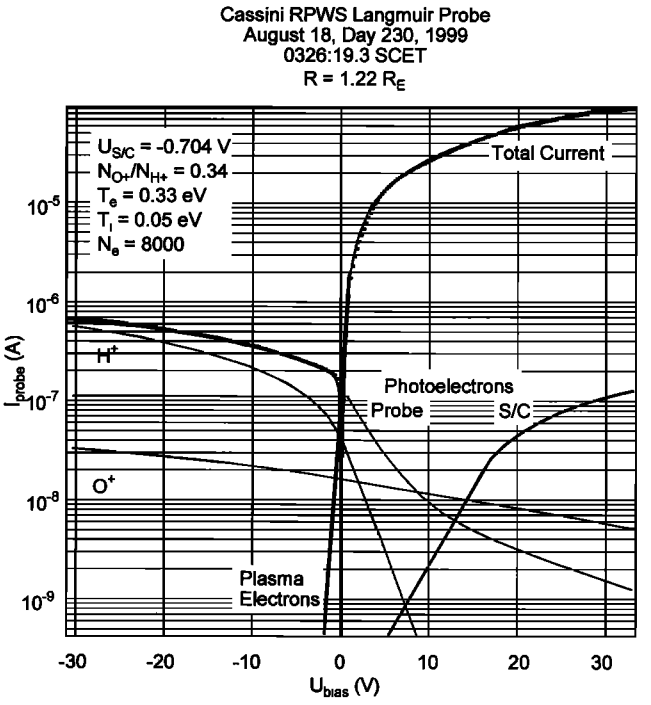

Figure 5. An example of a Langmuir probe sweep and associated modeling.

of the UV flux from the Sun. We estimate that the error in the determination of the electron density is ~10% and ~20% for the other parameters.

Electron densities determined from the Langmuir probe sweeps are shown in Figure 2 using solid triangles. The match with the density determined using the upper hybrid trace is guaranteed, since the Langmuir probe data were used to help determine the upper hybrid frequency in the spectrograms. This is a circular argument; however, the utility of having multiple sources of electron density information is clearly demonstrated here in that we were able to unambiguously identify f_{UH} in a complex spectrum. This would not have been possible to do in a convincing way without the supporting Langmuir probe data.

2.5. Planetary Radio Astronomy

As mentioned above, auroral kilometric radiation (AKR) was observed as a prominent component of the radio spectrum, particularly after closest approach when the spacecraft was near local midnight and well within the AKR emission cone [*Green et al.*, 1977; *Green and Gallagher*, 1985]. Some weak emission was seen inbound, but Cassini approached from the near-noon sector at low latitudes and hence was poorly situated to observe these auroral emissions. Plate 6 is a frequency-time spectrogram showing the occurrence of AKR from shortly after closest approach to the end of August 18. On the basis of the AKR measurements alone, it is clear that the magnetosphere was fairly disturbed and experienced a number of magnetic substorms during this interval. This conclusion is based on the long-established connection between the occurrence of AKR and discrete auroral arcs [*Gurnett*, 1974; *Huff et al.*, 1988] and the correlation between AE and the integrated power radiated in auroral kilometric radiation [*Voots et al.*, 1977; *Murata et al.*, 1997; *Kurth and Gurnett*, 1998; *Kurth et al.*, 1998].

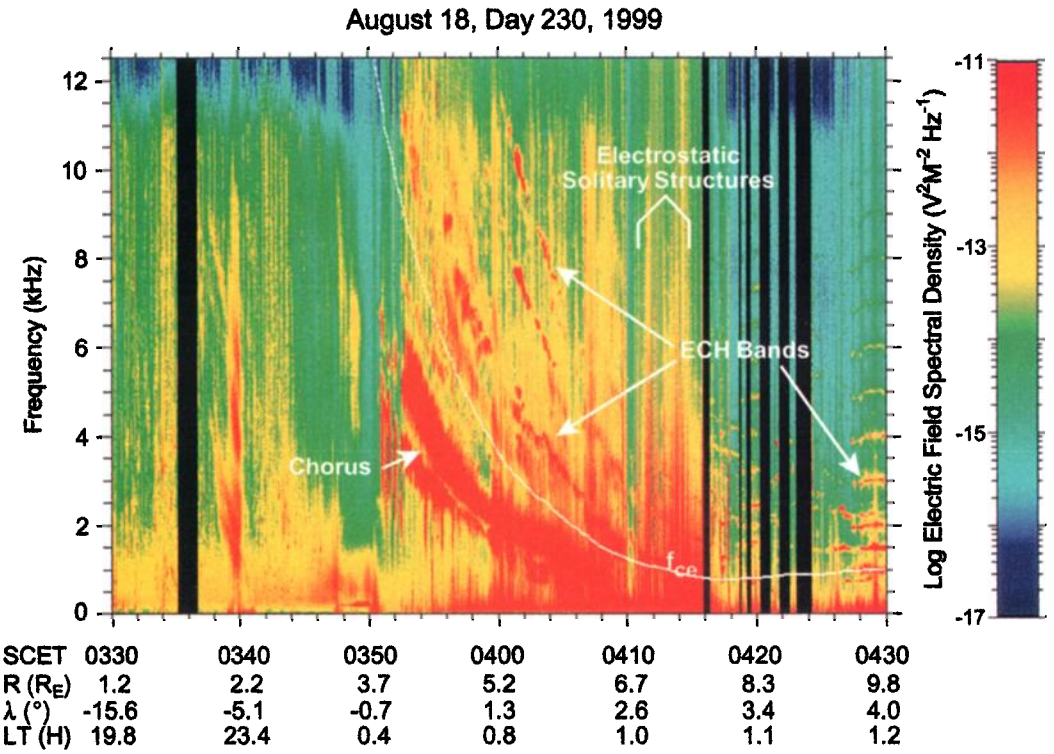

Plate 4. A wideband spectrogram showing details of chorus emissions and electron cyclotron harmonic emissions near the nightside plasmapause. Evidence for broadband electrostatic waves is also present.

Figure 6 shows the result of integrating the AKR spectrum once per minute from 50 to 800 kHz and scaling to a distance of 9 R_E as was done by *Kurth et al.* [1998]. The general rise in the integrated power flux seen particularly at the minima is simply due to the scaling; in effect, we are scaling the receiver background when there is no AKR signal in the integration bandwidth. A number of substorms are apparent in this display, although the situation becomes somewhat confusing in the time range between 1200 and 1800 SCET, where it is not clear whether there are multiple substorms being initiated before the previous one has dissipated or this is simply a prolonged, complex substorm. For simplicity we have adopted the former explanation. Table 1 presents the onset times for this series of substorms. For the first four events and the last event the onset time is quite clear; we simply take the time when the integrated flux begins to increase. For the period between 1200 and 1800 SCET we interpret the minima at 1433 and 1555 SCET as the onset times of new substorms.

Khan et al. [this issue] have studied the first two of these substorms globally and in great detail, including not only Cassini observations of these events but also incorporating a number of complementary ground-based and space-based observations for these. Included in that paper are detailed plots similar to Figure 6 but showing the correspondence between the AKR index and the expansion phase onset, the substorm intensification, the beginning of the recovery phase, and the end of the substorm disturbance. For these two substorms the onset of the expansion phase is nearly coincident with the initial jump in the AKR index. Both substorms also result in a subsequent increase in integrated AKR power flux at substorm intensification. There is also a marked decrease in AKR power flux which correlates reasonably well with the beginning of the recovery phase. By the end of the substorm disturbance the AKR index is very close to its background value. Hence the Cassini radio observations provide a good global assessment of magnetic activity through these two storms and confirm the utility of the integrated AKR power flux as a measure of magnetic activity when the spacecraft is suitably situated.

Beginning ~2 hours after closest approach, the high-frequency receiver was configured into a mode which enabled direction-finding and polarization measurements of auroral kilometric radiation. This operation provided an opportunity to run the instrument in a mode which will be used intensively near Jupiter, where a calibration will be done to determine the electrical orientations of the monopole antennas. This will be done by inverting the direction-finding analysis to use the known direction and polarization of Jovian radio emissions to determine the relative orientations and lengths of the antennas required to give the correct directions and polarization. We know from rheometry measurements [*Rucker et al.*, 1996] that the complex shape of the Cassini spacecraft rotates the electrical axes of the monopole antennas by several degrees from their physical orientations. Using direction finding of Jupiter when it appears as a point source (e.g., at distances greater than ~300 R_J), we can determine, in flight, these orientations. The goal is to achieve accuracies of order 1 degree for use in direction finding of Saturn radio emissions during tour. Preliminary analyses of the AKR direction finding indicate that both the electronics and the ground software provide reasonable solutions given that the Jupiter calibration has not yet occurred. A detailed analysis of the terrestrial data will be presented in a separate report.

While terrestrial radio emissions certainly dominated the radio spectrum during the Earth flyby, the RPWS instrument regularly observed Jovian radio emissions. In fact, *Kaiser et al.* [2000] have used these along with similar measurements from

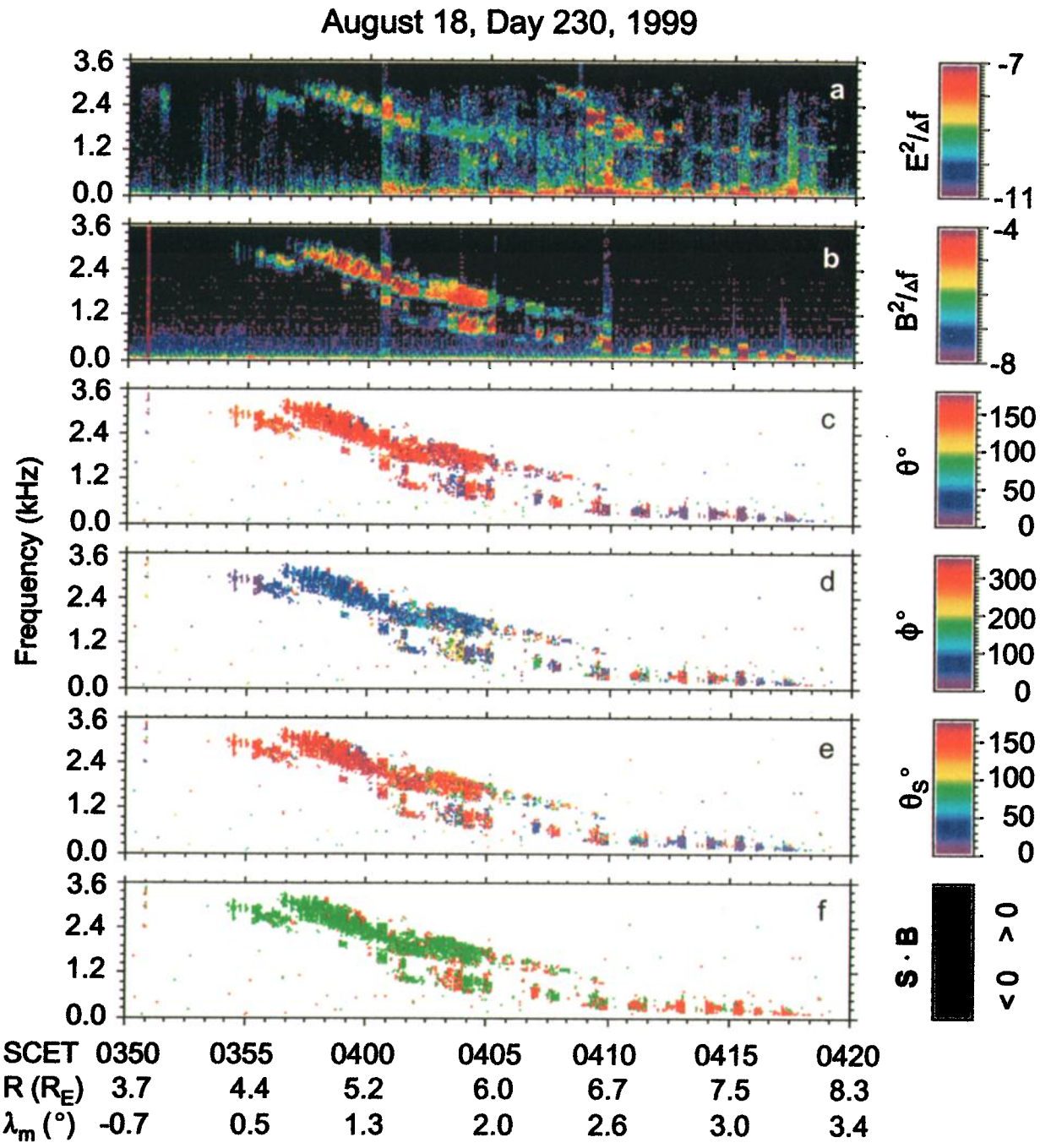

Plate 5. (a–f) A summary of the waveform receiver observations and results of analyses of wave normal direction and Poynting flux.

the Wind spacecraft to make the first stereoscopic estimates of the Jovian decametric radiation beam width (~1.5°) and to determine that Io-related decametric emissions rotate with Io's orbital period and not that of Jupiter. Plate 7 is an example of Jovian hectometric radiation at frequencies near 1 MHz observed by Cassini on September 7, 1999, when the spacecraft was more than 4 AU from Jupiter. The gap seen running through this example is a propagation effect recently explained by *Gurnett et al.* [1998] due to scattering of radio waves which propagate parallel to an L shell near that of Io. The detection of Jupiter from the vicinity of Earth and at signal-to-noise levels similar to those achieved by Wind suggests that the Cassini instrument's sensitivity is very good, given its 10-m antenna elements, and should be well equipped to thoroughly study Saturnian radio emissions. Furthermore, the Jupiter flyby will provide an unprecedented opportunity to perform a complete survey of the polarization characteristics of virtually all of the Jovian radio emissions.

In yet one more activity performed during the Earth flyby, two high-power HF radar stations (several hundred kilowatts) transmitted carrier signals toward Cassini and Wind. The goals of these transmissions are twofold. First, they provide a very localized radio source with known polarization characteristics with which to verify the Cassini RPWS polarization and direc-

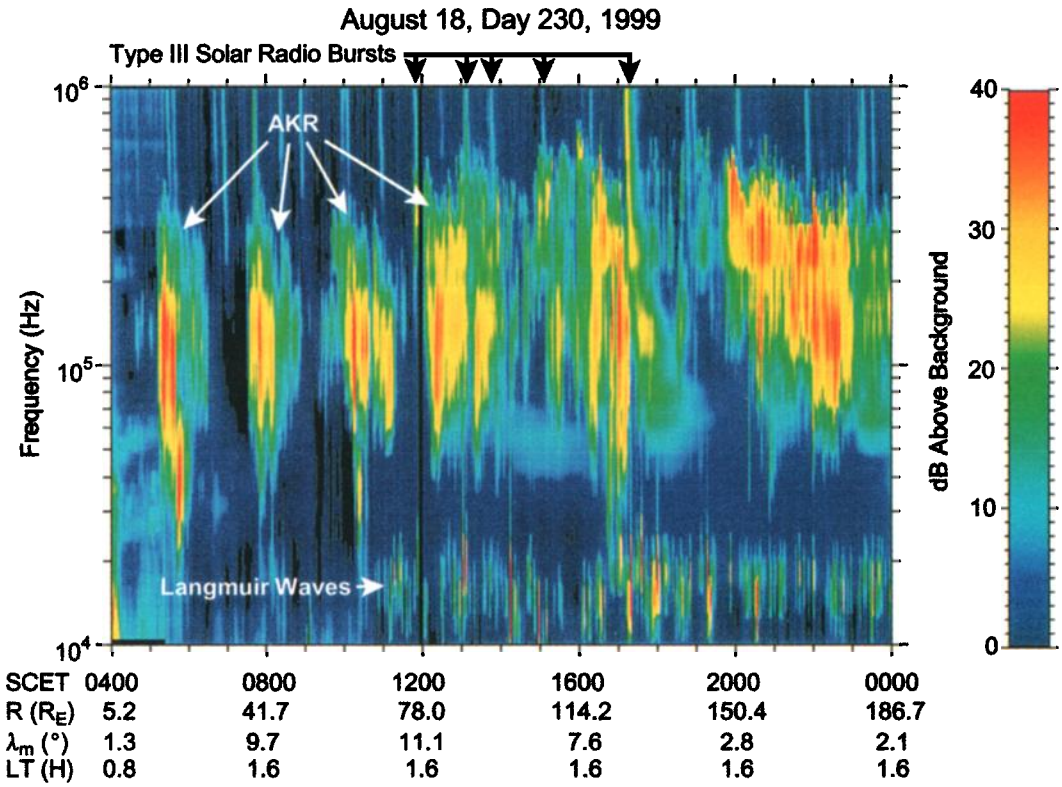

Plate 6. A series of auroral kilometric radiation (AKR) bursts indicating a series of magnetic substorms.

tion-finding measurements. Second, and perhaps primarily, the observations of the transmitted HF signals can be used to study large-scale density fluctuations in space plasmas. The two stations were SURA located near Nizhny Novgorod, Russia, and the High-Frequency Active Auroral Research Program (HAARP) facility near Gakona, Alaska, and transmitted when Cassini (and sometimes Wind) were in the field of view of the stations. The results of these experiments will be published elsewhere. However, as an example, in one experiment from the Russian station, both Wind (at a distance of 13.2 R_E) and Cassini (at a distance of 180 R_E) separated by only a few degrees as seen from the station received the signal transmitted at 9025 kHz. As expected, the ratio of the received power by the two spacecraft was inversely proportional to the square of the ratio of their respective distances. At 2230 UT the angular separation of the spacecraft seen from Earth was only ~1° increasing up to 7.5° near 2330 UT. Figure 7 shows the time variations of the SURA signal recorded by Cassini and Wind. As expected, the ratio of the received power by the two spacecraft was inversely proportional to the square of the ratio of their respective distances. Fluctuation spectra for Cassini and Wind were similar for the observed range of scintillation frequency (time sampling of 32 s).

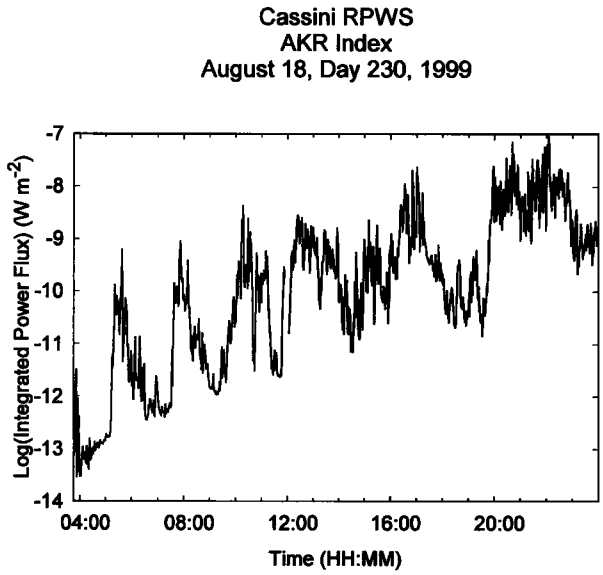

Figure 6. A plot of the auroral kilometric radiation power flux integrated from 50 to 800 kHz and scaled to 9 R_E. Previous studies have shown this quantity to be a reasonable proxy for the auroral electrojet index. Using this so-called AKR index, one can identify a number of individual substorms over this time interval.

Table 1. Substorm Onset Times for August 18, 1999, Based on Integrated AKR Power Flux[a]

Time, SCET	Comments
0511	clear onset time
0731	clear onset time
0926	beginning of gradual increase in activity
1146	clear onset time
1433	minimum between two substorms
1555	minimum between two substorms
1932	clear onset time

[a]SCET, spacecraft event time; AKR, auroral kilometric radiation.

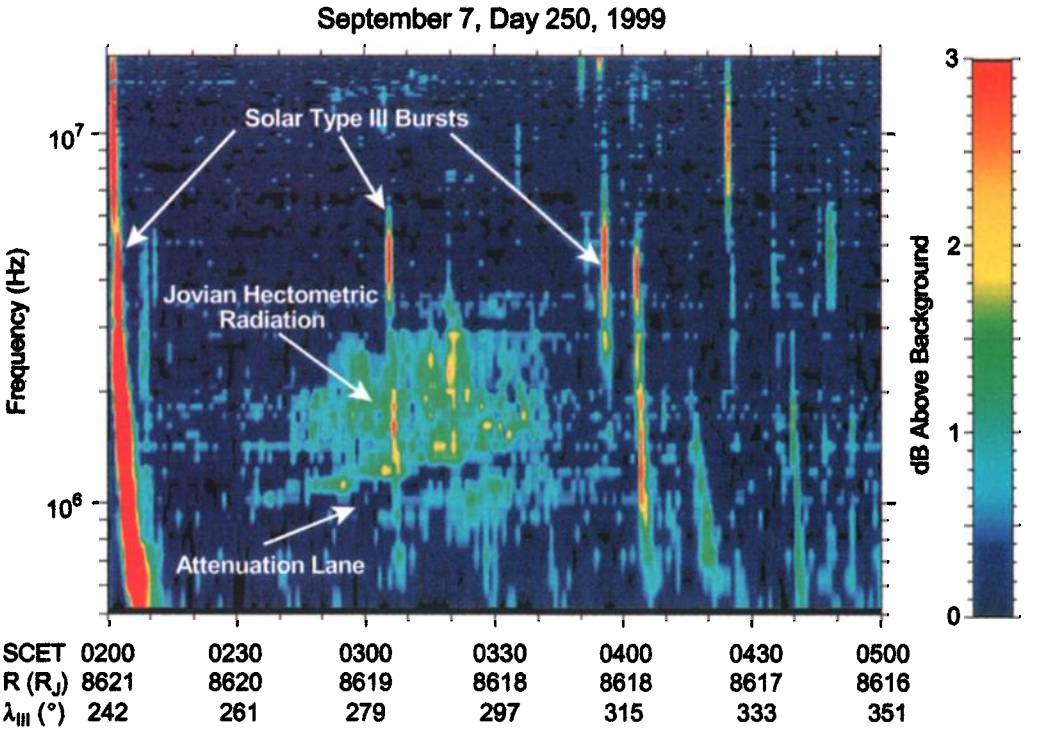

Plate 7. An example of a Jovian hectometric radiation event showing evidence of an attenuation lane believed to be a propagation effect near the L shell of Io.

3. Summary and Conclusions

This paper presents an overview of a comprehensive set of observations obtained during a swift flight through the terrestrial magnetosphere with a highly capable radio and plasma wave investigation on board the Cassini spacecraft. Since these were the first observations by this instrument within a planetary magnetosphere, the results are significant in showing the functionality of the overall instrument and the detailed operation of a number of its components. In addition, we present a plasma density profile from the dayside outer magnetosphere through the heart of the plasmasphere, electron phase space holes near the inner edge of the plasma sheet, and determine the direction of propagation and polarization of whistler mode chorus emissions which are consistent with recent reports using the Polar spacecraft.

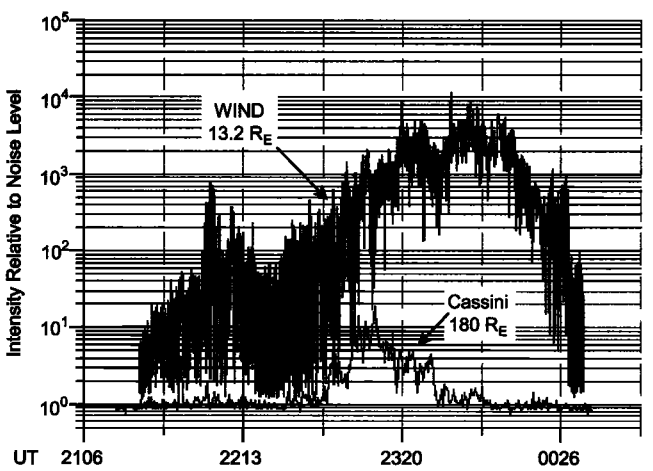

Figure 7. Intensity variations of the SURA signal at 9025 kHz recorded by the high-frequency receivers on the Cassini and Wind spacecraft on August 18–19, 1999.

The Cassini RPWS appears to be a very capable wave investigation. On the basis of the terrestrial flyby, the instrument shows both good noise characteristics and a wide dynamic range. Even with its relatively short antennas, the instrument detected continuum radiation trapped within the magnetosphere and on several occasions clearly observed Jovian radio emissions. Even with its low data rate survey receivers the instrument is capable of producing frequency-time spectrograms with spectral and temporal resolution sufficient to identify many of the common magnetospheric wave phenomena. Interference effects appear to be minimal, although it should be pointed out that the flyby was performed on reaction control system thrusters and not with reaction wheels for pointing and stabilization. On the basis of ground tests and analyses, we expect a modest level of magnetic interference at low frequencies from the reaction wheels at low frequencies. While the closest approach data did not include measurements below 25 Hz, because of an emphasis on higher-frequency whistler mode emissions, the instrument has a large analysis bandwidth extending from 1 Hz to 16 MHz.

An example of Jovian hectometric radiation was shown, demonstrating good sensitivity in the radio frequencies. A report has already been published showing the similarity of the sensitivity of this instrument with that of the Wind WAVES instrument [*Kaiser et al.*, 2000]. Not shown here but a product of the Earth flyby nevertheless are direction-finding measurements which were undertaken to validate this capability of the instrument and to prepare for a full antenna calibration during the Jupiter flyby in late 2000 and early 2001. Preliminary analyses show reasonable results from this portion of the instru-

ment although the accuracy suffers because of the lack of knowledge of the electrical orientation and relative lengths of the three monopole antennas.

Using a technique developed by both Geotail and Polar investigators, the integrated power flux of auroral kilometric radiation was calculated for the outbound leg of the flyby. This index shows a series of substorms which occurred from just after 0500 SCET through the end of August 18. The first two of these are studied in detail by *Khan et al.* [this issue] and show that there is a great deal of correspondence between the integrated power flux of AKR and the onset of the substorm expansion phase, the substorm intensification, the recovery, and the end of the substorm activity. Such correspondence is significant, since it is anticipated that similar observations of Saturn kilometric radiation will produce a magnetic activity index which will help to organize observations of magnetospheric dynamics during the Saturn tour.

A major objective of the flyby was to validate the capability of measuring the wave normal of whistler-mode emissions and to measure their Poynting flux. This objective was accomplished, and results on the propagation of whistler-mode chorus were obtained which are in agreement with a recent report by *LeDocq et al.* [1998]. That is, these emissions appear to propagate away from the magnetic equator, suggesting a source very close to the equator. These measurements, while straightforward in general, are fraught with possibilities for errors due to sensors being connected backward, input polarities being reversed, or phase shifts which are not properly calibrated. The possibilities for error extend to the analysis routines employed on the ground, where simple sign errors can invalidate the results. The Cassini measurements also require that the third electric field component be constructed from those which are measured and the assumption that $\mathbf{E} \cdot \mathbf{H} = 0$. It is not clear that this can be done reliably in all cases, but the results presented herein are certainly encouraging.

Both the sounder and the Langmuir probe were operated very briefly, but both operated as expected and were able to determine plasma densities which could stand on their own or be used to aid in the interpretation of the wave spectrum. The combined result is a density profile over much of the dayside and inner magnetosphere showing evidence for large detached regions of plasmasphere and strong density gradients on the plasmapause. This particular flyby revealed a relatively complex, two-banded spectrum near closest approach. Given the wave spectrum alone, there were some questions about how to identify the two bands. However, the independent determination of the electron density by the Langmuir probe allowed for the identification of a relatively broad band of Cerenkov radiation bounded at low frequencies by the electron plasma frequency and at high frequencies by the upper hybrid frequency. The higher-frequency band is the $5f_{ce}/2$ electron cyclotron harmonic band, just above $2f_{ce}$.

The high resolution afforded by the wideband receiver shows stunning spectral detail in a band of chorus and a set of electron cyclotron harmonic emissions on the nightside. These observations provide indications of broadband electrostatic noise. Inspection of the waveforms making up the wideband data set readily shows electrostatic solitary structures with timescales of 1 ms and amplitudes on the order of a few mV m^{-1}. This timescale is a few times slower than an electron plasma period and is consistent with an interpretation as electron phase space holes. The location of these observations is $\sim 7\ R_E$ in the tailward direction, near where one would expect the inner edge of the plasma sheet to be.

Acknowledgments. The research at the University of Iowa is supported by the National Aeronautics and Space Administration through contract 961152 through the Jet Propulsion Laboratory. Y.U.T. is grateful to CRDF for support (grant RP1-2107). We are grateful to D. Southwood and the Cassini magnetometer team for providing magnetic field measurements included. W.S.K. would like to acknowledge P. Kintner for useful discussions. Finally, the RPWS team would like to thank the men and women of the Cassini Program at the Jet Propulsion Laboratory for their skill and industry in carrying out this successful activity and affording the Cassini science investigations the opportunity to begin the process of understanding how to do science with this very capable spacecraft and its instruments.

Michel Blanc and Guest Editor Stanley Cowley thank Richard Horne and another referee for their assistance in evaluating this paper.

References

Ergun, R. E., et al., FAST satellite observations of large-amplitude solitary structures, *Geophys. Res. Lett.*, *25*, 2041–2044, 1998.

Franz, J. R., P. M. Kintner, and J. S. Pickett, Polar observations of coherent electric field structures, *Geophys. Res. Lett.*, *25*, 1277–1280, 1998.

Franz, J. R., P. M. Kintner, C. E. Seyler, J. S. Pickett, and J. D. Scudder, On the perpendicular scale of electron phase space holes, *Geophys. Res. Lett.*, *27*, 169–172, 2000.

Green, J. L., and D. L. Gallagher, The detailed intensity distribution of the AKR emission cone, *J. Geophys. Res.*, *90*, 9641–9649, 1985.

Green, J. L., D. A. Gurnett, and S. D. Shawhan, The angular distribution of auroral kilometric radiation, *J. Geophys. Res.*, *82*, 1825–1838, 1977.

Gurnett, D. A., The Earth as a radio source: Terrestrial kilometric radiation, *J. Geophys. Res.*, *79*, 4227–4238, 1974.

Gurnett, D. A., and L. A. Frank, A region of intense plasma wave turbulence on auroral field lines, *J. Geophys. Res.*, *82*, 1031–1050, 1977.

Gurnett, D. A., L. A. Frank, and R. P. Lepping, Plasma waves in the distant magnetotail, *J. Geophys. Res.*, *81*, 6059–6071, 1976.

Gurnett, D. A., J. D. Menietti, W. S. Kurth, and A. M. Persoon, An unusual rotationally modulated attenuation band in the Jovian hectometric radio emission spectrum, *Geophys. Res. Lett.*, *25*, 1841–1844, 1998.

Hospodarsky, G. B., T. F. Averkamp, W. S. Kurth, D. A. Gurnett, and M. Dougherty, Wave normal and Poynting vector calculations using the Cassini radio and plasma wave instrument, *J. Geophys. Res.*, this issue.

Hubbard, R. F., and T. J. Birmingham, Electrostatic emissions between electron gyroharmonics in the outer magnetosphere, *J. Geophys. Res.*, *83*, 4837–4850, 1978.

Hubbard, R. F., T. J. Birmingham, and E. W. Hones Jr., Magnetospheric electrostatic emissions and cold plasma densities, *J. Geophys. Res.*, *84*, 5828–5838, 1979.

Huff, R. L., W. Calvert, J. D. Craven, L. A. Frank, and D. A. Gurnett, Mapping of auroral kilometric radiation sources to the aurora, *J. Geophys. Res.*, *93*, 11,445–11,454, 1988.

Kaiser, M. L., M. D. Desch, J.-L. Bougeret, R. Manning, and C. A. Meetre, Wind/Waves observations of man-made radio transmissions, *Geophys. Res. Lett.*, *23*, 1287–1290, 1996.

Kaiser, M. L., P. Zarka, W. S. Kurth, G. B. Hospodarsky, and D. A. Gurnett, Cassini and Wind stereoscopic observations of Jovian nonthermal radio emissions: Measurement of beam widths, *J. Geophys. Res.*, *105*, 16,053–16,062, 2000.

Khan, H., et al., Observations of two complete substorm cycles during the Cassini Earth swing-by: Cassini magnetometer data in a global context, *J. Geophys. Res.*, this issue.

Krause, J. D., *Radio Astronomy*, pp. 116–130, McGraw-Hill, New York, 1966.

Kurth, W. S., Detailed observations of the source of terrestrial narrowband electromagnetic radiation, *Geophys. Res. Lett.*, *9*, 1341–1344, 1982.

Kurth, W. S., and D. A. Gurnett, Auroral kilometric radiation integrated power flux as a proxy for A_E, *Adv. Space Res.*, *22*(1), 73–77, 1998.

Kurth, W. S., J. D. Craven, L. A. Frank, and D. A. Gurnett, Intense electrostatic waves near the upper hybrid resonance frequency, *J. Geophys. Res.*, *84*, 4145–4164, 1979.

Kurth, W. S., T. Murata, G. Lu, D. A. Gurnett, and H. Matsumoto, Auroral kilometric radiation and the auroral electrojet index for the January 1997 magnetic cloud event, *Geophys. Res. Lett.*, *25*, 3027–3030, 1998.

LeDocq, M. J., D. A. Gurnett, and G. B. Hospodarsky, Chorus source locations from VLF Poynting flux measurements with the Polar spacecraft, *Geophys. Res. Lett.*, *25*, 4063–4066, 1998.

Matsumoto, H., H. Kojima, T. Miyatake, Y. Omura, M. Okada, I. Nagano, and M. Tsutsui, Electrostatic solitary waves (ESW) in the magnetotail: BEN wave forms observed by Geotail, *Geophys. Res. Lett.*, *21*, 2915–2918, 1994.

Means, J. D., Use of the three-dimensional covariance matrix in analyzing the polarization properties of plasma waves, *J. Geophys. Res.*, *77*, 5551–5559, 1972.

Murata, T., H. Matsumoto, H. Kojima, and T. Iyemori, Correlations of AKR index with K_p and D_{st} indices, *Proc. NIPR Symp. Upper Atmos. Phys.*, *10*, 64–68, 1997.

Rucker, H. O., W. Macher, R. Manning, and H. P. Ladreiter, Cassini model rheometry, *Radio Sci.*, *31*, 1299–1311, 1996.

Sagan, C., W. R. Thompson, R. Carlson, D. Gurnett, and C. Hord, A search for life on Earth from the Galileo spacecraft, *Nature*, *365*, 715–721, 1993.

Stokes, G., On the compositional resolution of streams of polarized light from different sources, *Trans. Cambridge Philos. Soc.*, *9*, 399–416, 1852.

Taylor, W. W. L., and S. D. Shawhan, A test for incoherent Cerenkov radiation for VLF hiss and other magnetospheric emissions, *J. Geophys. Res.*, *79*, 105–117, 1974.

Voots, G., D. A. Gurnett, and S.-I. Akasofu, Auroral kilometric radiation as an indicator of auroral magnetic disturbances, *J. Geophys. Res.*, *82*, 2259–2266, 1977.

P. Canu and A. Roux, CETP/UVSQ, F-92131, Velizy, France.

D. A. Gurnett, G. B. Hospodarsky, and W. S. Kurth, Department of Physics and Astronomy, University of Iowa, 203 Van Allen Hall, Iowa City, IA 52242-1479. (william-kurth@uiowa.edu)

M. L. Kaiser, Goddard Space Flight Center, Mail Code 695, Greenbelt, MD 20771.

Y. Tokarev, Radiophysical Research Institute (NIRFI), B. Pecherskaya Str., 25/14, 603950 Nizhny Novgorod, Russia.

J.-E. Wahlund, Swedish Institute of Space Physics, Uppsala Division, S-75591 Uppsala, Sweden.

P. Zarka, Observatoire de Paris, 5 Place Jules-Janssen, F-92195 Meudon, France.

(Received November 28, 2000; revised February 23, 2001; accepted February 24, 2001.)